# Two-stage sintering inhibits abnormal grain growth during $\beta$ to $\alpha$ transformation in SiC

Aaron M. Kueck and Lutgard C. De Jonghe

Materials Sciences Division, Lawrence Berkeley National Laboratory, and Department of Materials Science and Engineering, University of California, Berkeley, CA 94720, USA

## Abstract

Free sintering of SiC with Al, B, and C additions in two successive stages, first under nitrogen and then under argon, produced a near full-density ceramic with equiaxed grain structure. The $\beta$ to $\alpha$ transformation proceeded to completion; however, the grain shape remained equiaxed due to the action of nitrogen present during the first stage of sintering. It is found that the $\beta$ to $\alpha$ transformation is necessary but not sufficient for producing the microstructure of interlocking plates found in high toughness SiC.

## Introduction

SiC occurs in two general crystalline structures, the cubic $\beta$ form and the $\alpha$ polytypes. The most common $\alpha$ polytypes are 4H, 6H, and 2H which have hexagonal symmetry. At high temperatures $\beta$-SiC transforms to $\alpha$-SiC, stimulating grain growth and a change in grain shape from equiaxed to high aspect ratio plate-like. Grain size and shape are prime factors in determining the sintering behavior and, together with the nature of the grain boundaries,

determine the mechanical properties of SiC; thus, this transformation has been the focus of much study, *e.g.* the deeply probing work of Heuer and colleagues.[1-3]

Previous work has investigated means of manipulating the β to α transformation, including applied pressure[4-7], starting powder polytype composition[8-10], sintering aids[11-17], and sintering atmosphere[18-22]. For example, in the work by Zhang *et al.*[17] it was shown that the composition of a Al metal-B-C liquid phase forming additive significantly affected the resulting grain morphology, particularly depending on the Al content; the α SiC aspect ratio was reduced with decreasing Al content when hot-pressed in an Ar atmosphere. In another example, Suzuki *et al.*[22] and Padture and colleagues[20,21] found that a nitrogen atmosphere can completely suppress the β−α transformation while argon enhances it. In a related paper, Deshpande *et al.*[23] argued that annealing in nitrogen reduced the planar defect concentration in β-SiC, and thus removed nucleation sites for the β−α transformation. Enhanced solution-precipitation and transport rates in liquid-phase sintering generally favor densification as well as rapid transformation and grain growth; however, rapid grain growth can result in early impingement of large grains, forming a skeleton that effectively arrests densification in free sintering. Here we report on the effects of a two-stage dual atmosphere free sintering of a SiC containing Al, B and C sintering aids, at 1900ºC, whereby the initial $N_2$ atmosphere is changed to an Ar one. This two-step process frustrates abnormal grain growth, yet does not inhibit either the β−α transformation or the normal grain growth process, leading to a sintered body with densities in excess of 95% of theoretical, with an equiaxed α SiC grain structure.

## Methods

Submicron β-SiC powder (Betarundum, Grade ultrafine, IBIDEN, Japan), with a mean particle size of 0.27 μm, was mixed with 3 wt% Al metal, 0.6 wt% B and 2 wt% C additives in cyclohexane (3ABC-SiC). This composition can lead to a high-toughness SiC when hot-pressed due to the retention of a nanoscale intergranular phase that promotes grain boundary crack paths.[16] The Al powder (H-3, Valimet, Stockton, CA) had an average size of 3 μm. The boron powder (Alfa Aesar) had a particle size of less than 5 μm. The carbon was introduced as Apiezon wax, which has a conversion yield of about 50wt% C.[16] The slurry was ultrasonically agitated, stir-dried and sieved through a 200 mesh screen. 1.2 cm diameter pellets were formed by uniaxial pressing in a steel die at 140 MPa.

Samples, packed in powder of the same nominal composition in a graphite crucible lined with graphite foil, were sintered in a graphite resistance furnace. The first sintering step was performed under flowing nitrogen (~1 atm) at 1900ºC, for 5 hours. After the first step, the samples were removed, weighed and the dimensions measured, packed in fresh powder, and sintered for an additional 4 hours at 1900ºC, under a flowing argon atmosphere.

Mechanical properties were assessed by Vickers microindentation using loads of 9.8 or 98 N (1 or 10 kg). Ten indents were made for each measurement. Hardness and indentation toughness were calculated using the equations:

$$H = 1.854 \left( \frac{P}{d^2} \right)$$

$$K_c = 0.016\left(\frac{E}{H}\right)^{1/2}\left(\frac{P}{c^{3/2}}\right)$$

where H is the hardness, P is the indentation load, E is the elastic modulus (assumed to be 390 GPa), $K_c$ is the indentation toughness, and d and c are the indent diagonal length and the crack length, respectively.[24]

Microstructural analysis was performed using optical, scanning electron (SEM), and transmission electron microscopy (TEM). To produce contrast in the SEM (JEOL JSM-6340F), samples were etched in a plasma of $CF_4$ with 4% $O_2$, for 20-60 minutes. Samples for the TEM were prepared by grinding, dimpling, and argon ion milling at 5 kV. Nanoprobe energy dispersive spectroscopy (EDS) was performed using a Philips CM200/FEG. Lattice images were produced using a Philips CM300FEG/UT at 300 kV operating voltage.

Crystal structures were determined by least-squares fitting of x-ray diffraction data to the equations of Ruska *et al.*[25]

## Results

Sintering behavior

During the 5 h first sintering at 1900°C under a nitrogen atmosphere, densification leveled off at about 85% of the theoretical density, with a microstructure shown in Figure 1. A few

areas in this sample contained features that were interpreted as residuals of a liquid phase that was present during this first sintering step. These residual liquid phases had an approximate composition of $SiAlCN_2$ with <5 at% O, based on semi-quantitative EDS analysis, Fig. 2, of such a feature. Individual particles in this sample were up to 1 µm in size. XRD analysis, Fig. 3, confirmed the complete suppression of the transformation from cubic to hexagonal structure, as expected. Although there was evidence of the presence of a liquid phase, densification did not proceed beyond the 85% mentioned above.

EDS analysis estimated that on average about 1.5 wt% N was absorbed into the specimens during the first sintering step. This is consistent with a reduced weight loss compared to that for argon sintering under similar conditions, of about 2 wt% (sintering in argon produced a weight loss of 5 wt%; under nitrogen the weight loss was only 3 wt%). In addition to being readily absorbed into a liquid phase, nitrogen enriched the grain boundaries. Nanoprobe EDS measured a nitrogen concentration of 7.4 wt% at the boundary compared to an average of 1.0 wt% at grain centers. Aluminum was similarly concentrated at grain boundaries, with 4.3 wt% present compared to 2.2 wt% at grain centers.

The second sintering stage, now under argon, produced dramatic changes in the microstructure. Liquid phase sintering occurred during the first hour, increasing the density to about 90%. Further coarsening and densification brought the final density to about 95%. As a result of the liquid phase, the grain structure transformed to 100% hexagonal, about

90% 4H. This polytype content is nearly identical to that of a hot-pressed SiC of similar composition.[16]

The grain morphology, despite a hexagonal crystal structure, remained equiaxed, and grain boundaries were curved instead of faceted. [Figure 4] Furthermore, the average grain size of 5 μm was much finer than 3ABC-SiC free-sintered under argon, which reached 50-100 μm after 10 hours at 1825ºC. Residual second phases were not observed with SEM; EDS and EELS traces could not detect the typical enrichment of Al and N at the grain boundaries, suggesting the lack of a grain boundary phase. TEM confirmed that nearly all the grain boundaries were free of an intergranular film. [Figure 5] Table 1 summarizes the average concentrations of N and Al before and after the argon sintering step.

Indentation properties

Microindentation was used to compare the two-step sintered specimens to traditional hot-pressed 3ABC-SiC. Residual porosity of ~5% caused the indentation properties to vary substantially with indentation load. Higher loads sampled more of the pores, causing the apparent hardness to decrease and the apparent indentation toughness to increase. The toughness increases with indentation load because the pores act to blunt cracks and increase the compliance; more interaction of the crack with pores causes the crack to be shortened, thus increasing the measured toughness. Table 2 summarizes the indentation mechanical properties of dual atmosphere sintered 3ABC-SiC, with values for hot-pressed 3ABC-SiC given for reference.

## Discussion

Table 3 highlights the major events that occur during the two-step sintering process.

EDS analysis showed that, on average, approximately 2 at% N is incorporated into the samples during the heat treatment under nitrogen, similar to absorbed amounts in another study.[20] Absorption preferentially occurs in the liquid phase when it is present, due to higher $N_2$ solubility in this phase[19,20]; this is clearly seen in the approximate liquid composition of $SiAlCN_2$. In the liquid, nitrogen has two important effects. First, as expected, it reduces the liquid volume fraction during the first step and slows transport through the liquid[20,21], reducing grain growth and producing a finer microstructure.[20] Second, as expected, it enhances the stability of the cubic phase while a nitrogen source is provided.[19,20] The presence of nitrogen in the grain boundaries also roughens the grain surfaces, eliminating the grain growth anisotropy during the second sintering step that would arise from faceting.[19,26-29] Lack of faceting can be seen in the curved grain boundaries of Figure 4.

During the treatment in argon, the absorbed nitrogen was lost. This allowed the formation of an active liquid phase that completed the sintering during the first hour. Then, nitrogen and aluminum were lost while the liquid phase escaped. This is thought to give rise to the intriguing features that can be found near the grain boundaries of the polished and etched samples. These grain boundary regions appear brighter than the grain centers, and are 100-

200 nm below the centers after etching, as measured by stereograms. They appear to show a "record" of the grain boundary movements. [Fig 4 a and 4b] EDS and EELS find that these regions have a measurably lower Al/Si ratio, with decreasing aluminum content as the grain boundary sweeps further into the adjacent grain. It is tempting to speculate that the grain boundary movement involves some residual liquid phase, originally rich in Al, that is progressively lost by evaporation from the boundary as the grain boundary advances, leaving a wake of SiC lower in Al content.

It is also interesting to note that the transient nature of the liquid phase did not suppress the β-α transformation, as was the case demonstrated by Stutz *et al.*[30]. In that case, the liquid was partially removed before the structural transformation, which retarded densification and transformation. Here the liquid is removed after densification, which allows for a lower processing temperature and complete conversion to the hexagonal structure. In both cases, however, the grain structure remains predominantly fine-grained and equiaxed. While Stutz *et al*. prevented abnormal growth by preemptively removing the liquid, here the liquid composition is altered to prevent grain faceting.

TEM investigation confirmed that at the end of the second sintering treatment in Ar, the large majority of grain boundaries show no evidence of secondary crystalline or amorphous intergranular films.  [Figure 5] Since the weight loss during the second sintering step is less than the amount of nitrogen absorbed during the first step, it is possible that some nitrogen remains at these locations. However, EDS and EELS analysis measures the total N content

as zero and can find no N signals in grain boundaries, indicating that nitrogen, if present, exists at very low concentrations. Without residual liquid phase, there are a majority of clean "dry" boundaries. The lack of a liquid phase at the end of sintering is further indicated by the slightly increased etch rates near many grain boundaries.[26,31]

Despite the loss of nitrogen during evaporation of the liquid phase, grain boundaries did not facet, indicating a nonreversible effect of the nitrogen treatment. Levels of nitrogen were low enough to allow the transformation to hexagonal structure, but not low enough for the grain surfaces to facet and abnormal growth to occur. The lack of abnormal grain growth results in an equiaxed grain structure of hexagonal grains. Whereas previous work, such as that of Padture *et al.*[20,21], found that the β-α transformation was necessary for producing high-toughness SiC, here we find that this is not a sufficient condition. The growth of *faceted* hexagonal grains produces the network of interlocking platelike grains; pretreatment in a nitrogen atmosphere prior to liquid phase sintering in argon is enough to disrupt the faceting without preventing the transformation from cubic to hexagonal structure.

## Conclusion

SiC, doped with Al, B,and C, was free-sintered in two stages, first under $N_2$ and then under Ar. By providing a source of nitrogen, faceting and abnormal grain growth that accompanies the cubic to hexagonal transformation in SiC sintered under argon, was prevented. The modification of grain surfaces by nitrogen during sintering prevented facets

from forming on newly precipitated hexagonal grains. Without facets, grains grew into equiaxed shapes; this indicates that the β-α transformation is necessary but not sufficient to produce SiC with high aspect ratio grains for enhanced toughness.

## Acknowledgements

## References

1.	Heuer, A. H., Fryburg, G. A., Ogbuji, L. U.,  Mitchell, T. E., & Shinozaki, S., β→α transformation in polycrystalline SiC: I. J. Am. Ceram. Soc., 1978, 61, 406-412.

2.	Mitchell, T. E., Ogbuji, L. U., & Heuer, A. H., β-α transformation in polycrystalline SiC: II. J. Am. Ceram. Soc., 1978, 61, 412-413.

3.	Ogbuji, L. U., Mitchell, T. E., & Heuer, A. H., β-α transformation in polycrystalline SiC: III, the thickening of α plates. J. Am. Ceram. Soc., 1981, 64, 91-99.

4. Xie, R. J., Mitomo, M., Kim, W., Kim, Y. W., Zhan, G. D., & Akimune, Y., Phase transformation and texture in hot-forged or annealed liquid-phase-sintered silicon carbide ceramics. J. Am. Ceram. Soc., 2002, 85, 459-465.

5. Zhan, G. D., Mitomo, M., Tanaka, H., & Kim, Y. W., Effect of annealing conditions on microstructural development and phase transformation in silicon carbide. J. Am. Ceram. Soc., 2000, 83, 1369-1374.

6. Zhan, G., Xie, R., & Mitomo, M., Effect of $\beta$-to-$\alpha$ phase transformation on the microstructural development and mechanical properties of fine-grained silicon carbide ceramics. J. Am. Ceram. Soc., 2001, 84, 945-950.

7. Zhan, G., Ikuhara, Y., Mitomo, M., Xie, R., Sakuma, T., & Mukherjee, A. K., Microstrucural analysis of liquid-phase-sintered $\beta$-silicon carbide. J. Am. Ceram. Soc., 2002, 85, 430-436.

8. Zhan, G., Mitomo, M., & Kim, Y., Microstructural control for strengthening of silicon carbide ceramics. J. Am. Ceram. Soc., 1999, 82, 2924-2926.

9. Tanaka, H., Hirosaki, N., Nishimura, T., Shin, D. W., & Park, S. S., Nonequiaxial grain growth and polytype transformation of sintered $\alpha$-silicon carbide and $\beta$-silicon carbide. J. Am. Ceram. Soc., 2003, 86, 2222-2224.

10. Lee, C. S., Kim, Y. W., Cho, D. H., Lee, H. B., & Lim, H. J., Microstructure and mechanical properties of self-reinforced alpha-silicon carbide. Ceramics International, 1998, 24, 489-495.

11.    Nagano, T., Gu, H., Kaneko, K., Zhan, G. D., & Mitomo, M., Effect of dynamic microstructural change on deformation behavior in liquid-phase-sintered silicon carbide with $Al_2O_3$-$Y_2O_3$-CaO additions. J. Am. Ceram. Soc., 2001, 84, 2045-2050.

12.    Rixecker, G., Biswas, K., Rosinus, A., Sharma, A., Wiedmann, I., & Aldinger, F., Fracture properties of SiC ceramics with oxynitride additives. J. Eur. Ceram. Soc., 2002, 22, 2669-2675.

13.    Lee, S., Kim, Y., & Mitomo, M., Relationship between microstructure and fracture toughness of toughened silicon carbide ceramics. J. Am. Ceram. Soc., 2001, 84, 1347-1353.

14.    Zhou, Y., Hirao, K., Toriyama, M., Yamauchi, Y., & Kanzaki, S., Tailoring the mechanical properties of silicon carbide ceramics by modification of the intergranular phase chemistry and microstructure. J. Eur. Ceram. Soc., 2002, 22, 2689-2696.

15.    Zhou, Y., Hirao, K., Toriyama, M., Yamauchi, Y., & Kanzaki, S., Effects of intergranular phase chemistry on the microstructure and mechanical properties of silicon carbide ceramics densified with rare-earth oxide and alumina additions. J. Am. Ceram. Soc., 2001, 84, 1642-1644.

16.    Cao, J. J., Moberlychan, W. J., DeJonghe, L. C., Gilbert, C. J., & Ritchie, R. O., In-situ toughened silicon carbide with Al-B-C additions. J. Am. Ceram. Soc., 1996, 79, 461–469.

17.    Zhang, X. F., Yang, Q., & DeJonghe, L. C. Microstructure development in hot-pressed silicon carbide: effects of aluminum, boron, and carbon additives. Acta Materialia, 2003, 51, 3849-3860.

18.    Nagano, T., Kaneko, K., Zhan, G. D., & Mitomo, M., Effect of atmosphere on weight loss in sintered silicon carbide during heat treatment. J. Am. Ceram. Soc., 2000, 83, 2781-2787.

19.    Jang, C. J., Kim, J., & Kang, S. L., Effect of sintering atmosphere on grain shape and grain growth in liquid-phase-sintered silicon carbide. J. Am. Ceram. Soc., 2002, 85, 1281-1284.

20.    Ortiz, A. L., Bhatia, T., Padture, N. P, & Pezzotti, G., Microstructural evolution in liquid-phase-sintered SiC: part III, effect of nitrogen-gas sintering atmosphere. J. Am. Ceram. Soc., 2002, 85, 1835-1840.

21.    Ortiz A. L., Munoz-Bernabe A., Borrero-Lopez O., Domınguez-Rodrıguez A., Guiberteau F., & Padture N. P., Effect of sintering atmosphere on the mechanical properties of liquid-phase-sintered SiC. J. Eur. Ceram. Soc., 2004, 24, 3245-3249.

22.    Suzuki, K. & Sasaki, M., Effects of sintering atmosphere on grain morphology of liquid-phase-sintered SiC with $Al_2O_3$ additions. J. European Ceramic Society, 2005, 25, 1611–1618.

23.    Deshpande, S. A., Bhatia, T., Xu, H., Padture N. P., Ortiz, A. L., & Cumbrera, F. L., Microstructural evolution in liquid-phase-sintered SiC: Part II, effects of planar defects and seeds in the starting powder. J. Am. Ceram. Soc., 2001, 84, 1585-1590.

24.    Chantikul, P., Anstis, G. R., Lawn, B. R., & Marshall, D. B., A critical evaluation of indentation techniques for measuring fracture toughness: II, strength method. J. Am. Ceram. Soc., 2001, 64, 539-543.

25.   Ruska, J., Gauckler, L. J., Lorenz, J. L., Rexer, H. U., The quantitative calculation of SiC polytypes from measurements of x-ray diffraction peak intensities. J. Materials Science, 1979, 14, 2013-2017.

26.   Ye, H., Pujar, V., & Padture, N., Coarsening in liquid-phase-sintered $\alpha$-SiC. Acta Mat., 1999, 47, 481-487.

27.   Kim, Y. W., Mitomo, M., & Zhan, G. D., Mechanism of grain growth in liquid-phase-sintered $\beta$-SiC. J. Mater. Research, 1999, 14, 4291-4293.

28.   Wijesundara, M. B. J., Stoldt, C. R., Carraro, C., Howe, R. T., & Maboudian, R. Nitrogen doping of polycrystalline 3C–SiC films grown by single-source chemical vapor deposition. Thin Solid Films, 2002, 419, 67-75.

29.   Wijesundara, M. B. J., Gao, D., Carraroa, C., Howe, R. T., & Maboudian, R. Nitrogen doping of polycrystalline 3C-SiC films grown using 1,3-disilabutane in a conventional LPCVD reactor. J. Crystal Growth, 2003, 259, 18-25.

30.   Stutz, D. H., Prochazka, S., & Lorenz, J. Sintering and microstructure formation of $\beta$-silicon carbide. J. Am. Ceram. Soc., 1985, 68, 479-482.

31.   Sigl, L., & Kleebe, H. J., Core/rim structure of liquid-phase-sintered silicon carbide. J. Am. Ceram. Soc., 1993, 76, 773-776.

Table 1: Average N and Al content (in wt%) of 3ABC-SiC after each

step in the two-step sintering process.

|  | After first step in $N_2$ | After second step in Ar |
|---|---|---|
| N | 1.5 +/- 0.2 | 0 |
| Al | 3.7 +/- 0.1 | 3.1 +/- 0.1 |

Table 2: Indentation properties of 3ABC-SiC

| Processing | Indentation Load (kg) | Hardness (GPa) | Indentation Toughness (MPa√m) | Crack Path |
|---|---|---|---|---|
| Two-step pressureless | 1 | 20.4 ± 1.2 | 2.5 ± 0.5 | Transgranular |
| Two-step pressureless | 10 | 17 ± 6 | 3.7 ± 0.7 | Transgranular |
| Hot press | 10 | 18 ± 2 | 6 ± 1 | Intergranular |

Table 3: Important events during two-stage sintering of 3ABC-SiC

| | | | |
|---|---|---|---|
| **Stage 1: Nitrogen atmosphere, 5 hours** | A liquid phase forms above 1825ºC. | Moderate densification occurs. | Nitrogen is absorbed, primarily in the liquid and grain boundaries. |
| **Stage 2: Argon atmosphere, first 30 minutes** | Nitrogen begins to desorb and escape the system. | A lower viscosity liquid forms as N escapes. | Traditional liquid phase sintering and cubic-hexagonal transformation begin. |
| **Stage 2: Argon atmosphere, after 1 hour** | Liquid phase sintering nearly complete. | β-α transformation nearly complete. | |
| **Stage 2: Argon atmosphere, after 4 hours** | Liquid phase sintering complete, final density reached. | β-α transformation complete. | Liquid phase has completely evaporated. |
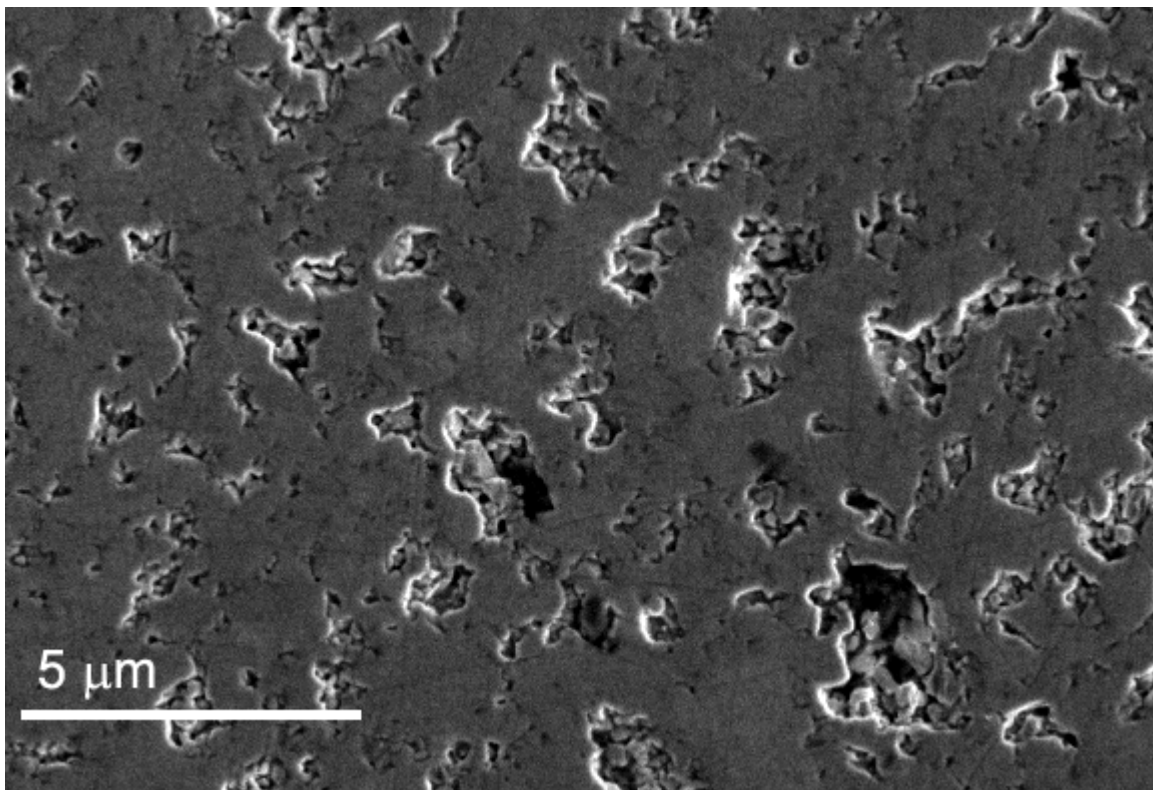
Figure 1: SEM image of 3ABC-SiC pressureless sintered under nitrogen at 1900℃ for 5

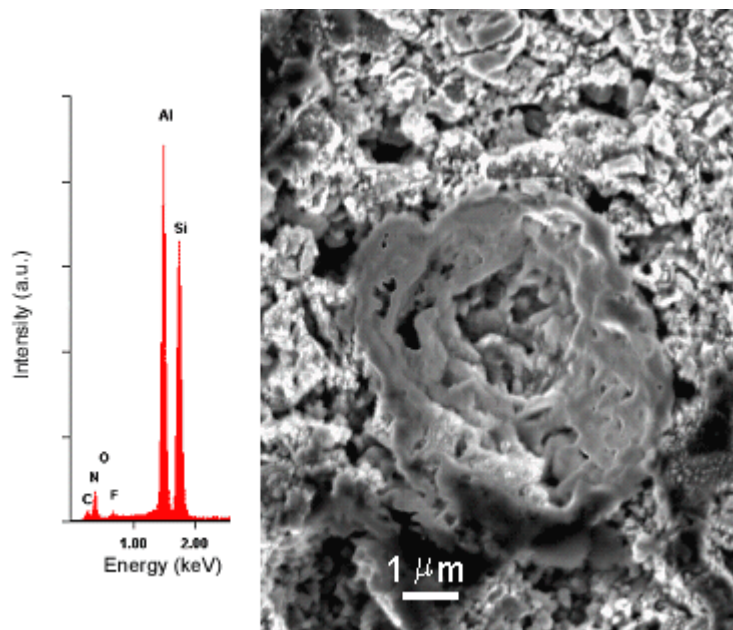hours. Individual particles range in size from 300nm to 1µm.

Figure 2: EDS spectrum (left) of liquid phase (right) present after pre-sintering in nitrogen.

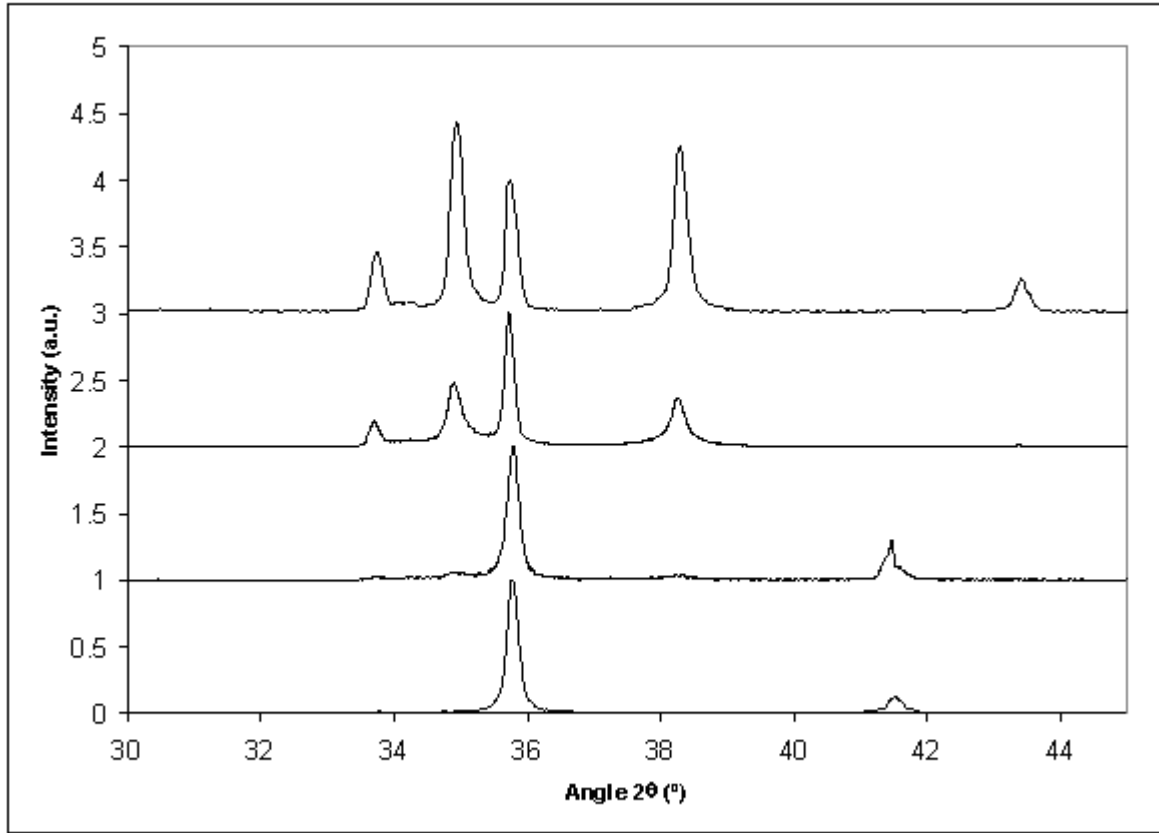The F peak results from fluorine attachment during the etching process.

Figure 3: X-ray diffraction scans of 3ABC-SiC after the first sintering step in nitrogen (bottom), after 30 minutes in Ar, 1 hour in Ar, and 4 hours in Ar (top). The first step completely suppresses the β to α transformation, which occurs mostly between 30 mins and 1 hour in Ar and is complete at 4 hours. The $<111>_\beta/<0001>_\alpha$ peaks have been normalized to a height of 1.
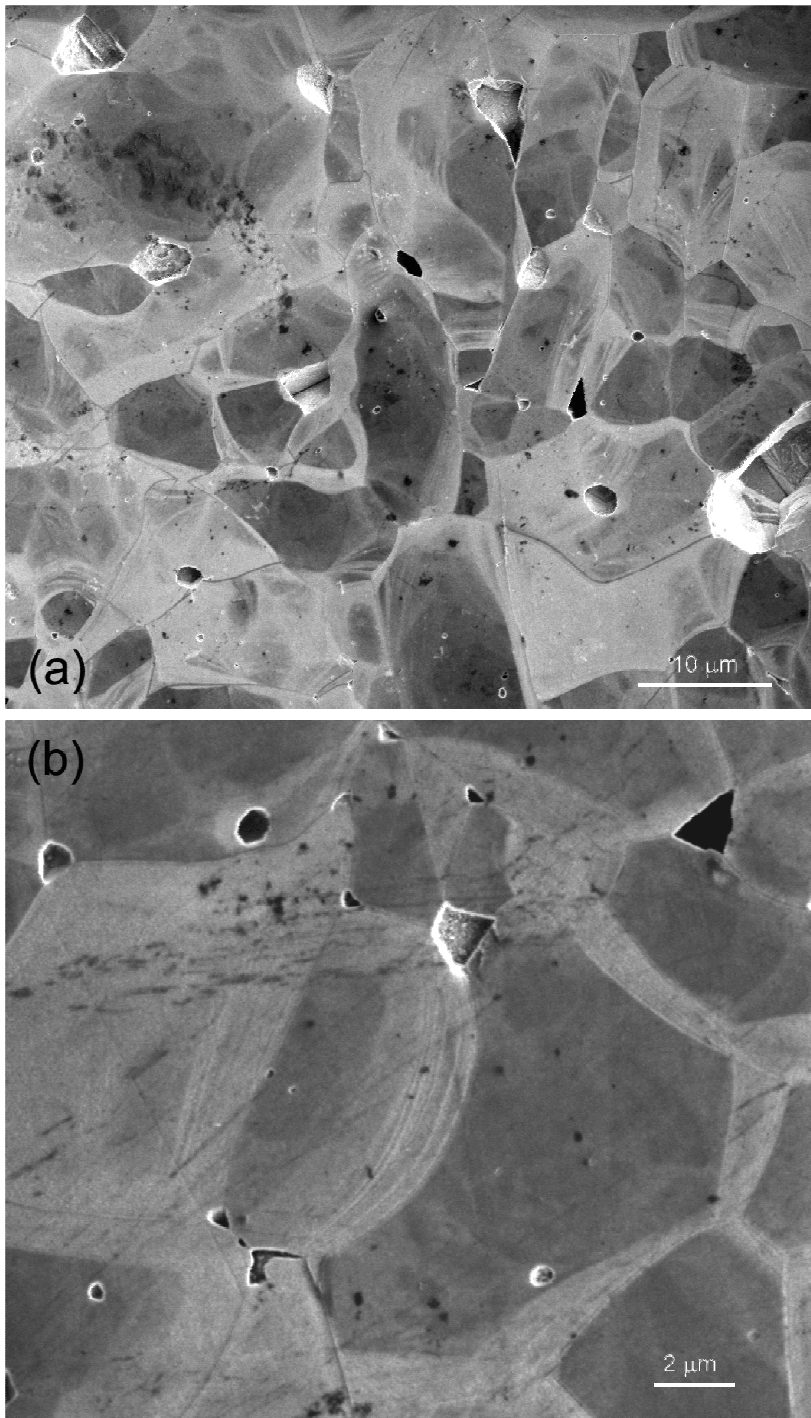
Figure 4: SEM images of 3ABC-SiC two-step pressureless sintered: 1900ºC 5hrs under nitrogen plus 1900ºC 4 hours under argon. Plasma etched to show grain boundaries. Note the equiaxed grain shapes and the curved grain boundaries.
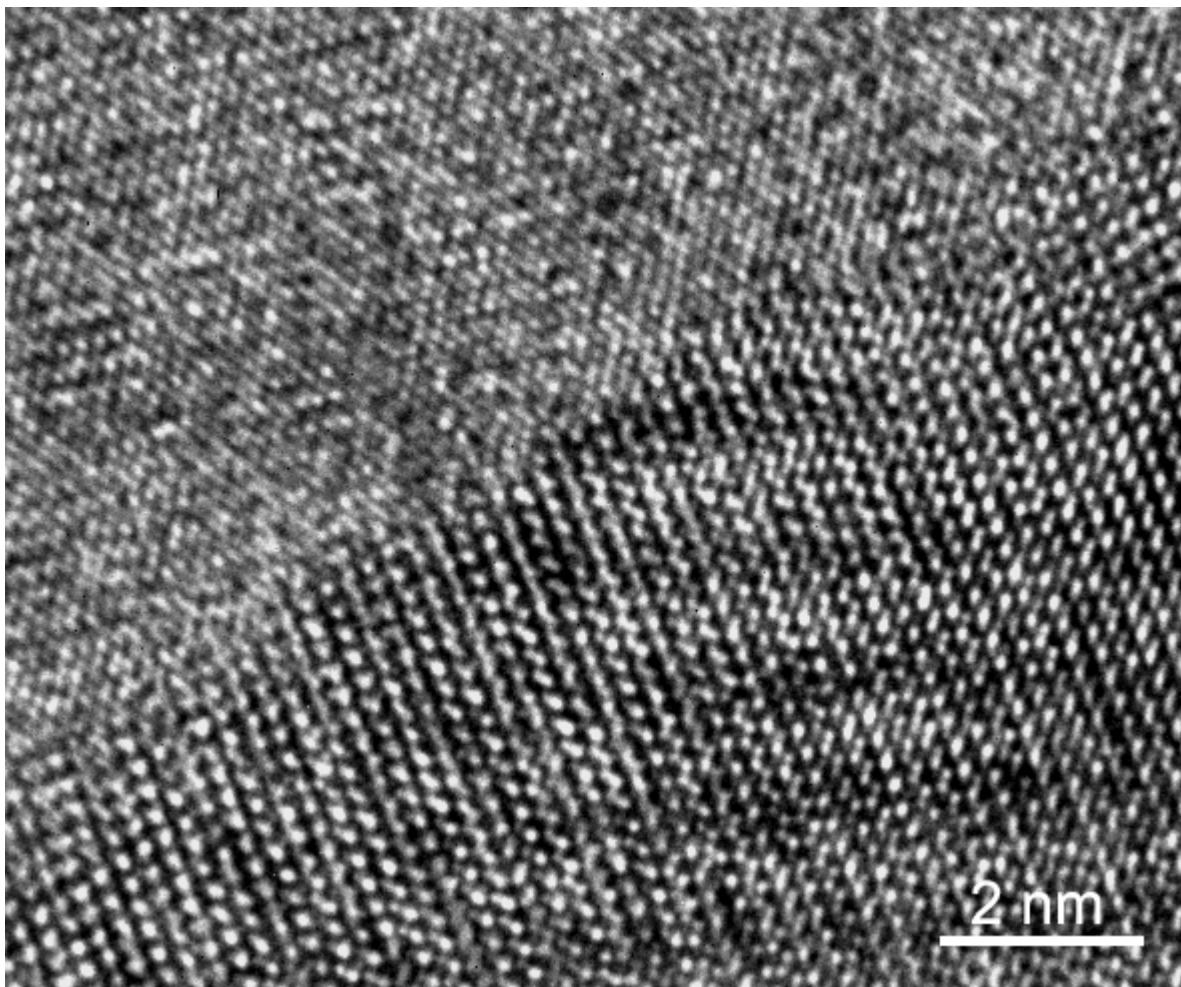
Figure 5: Transmission electron micrograph of a typical grain boundary in two-step pressureless sintered 3ABC-SiC. No intergranular film is present along the boundary. Bar at lower right is 2 nm.